Measurement of Elastic Electron-Neutron Cross Sections up to $Q^2 = 10$ (GeV/c)^2

S. Rock, R. G. Arnold, P. Bosted, B. T. Chertok,[a] B. A. Mecking,[b] I. Schmidt,[c] Z. M. Szalata, R. C. York,[d] and R. Zdarko

Department of Physics, The American University, Washington, D.C. 20016, and Stanford Linear Accelerator Center, Stanford University, Stanford, California 94305

(Received 7 September 1982)

The elastic electron-neutron cross section has been measured at four-momentum transfers squared (Q^2) of 2.5, 4.0, 6.0, 8.0, and 10.0 (GeV/c)^2 with use of a deuterium target and detection of the scattered electrons at 10°. The ratio of neutron to proton elastic cross sections decreases with Q^2. At high Q^2 this trend is inconsistent with the dipole law, form-factor scaling, and many vector dominance models, although it is consistent with some parton models.

PACS numbers: 25.30.Cq, 13.40.Fn, 27.10.+h

Determining the structure of the nucleons is one of the fundamental problems of physics. A wide variety of empirical and theoretical models ranging from form-factor scaling[1] and vector dominance[2] to quark-parton models[3] and perturbative QCD[4] have been used to explain the elastic cross sections (σ_p, σ_n). Most of the current models agree with existing data but diverge from each other in the previously unexplored region of high four-momentum transfer squared (Q^2). While σ_p has been measured[5] up to $Q^2 = 33$ (GeV/c)^2, σ_n had been reliably measured[6] only to $Q^2 = 4$ (GeV/c)^2. Here we report measurements of σ_n out to $Q^2 = 10.0$ (GeV/c)^2.

The cross section for elastic electron-nucleon scattering can be written as

$$d\sigma/d\Omega = \sigma_{\rm M}[A(Q^2) + B(Q^2)\tan^2(\tfrac{1}{2}\theta)], \qquad (1)$$

where $\sigma_{\rm M}$ is the Mott cross section, $A = (G_E^{\,2} + \tau G_M^{\,2})/(1+\tau)$, and $B = 2\tau G_M^{\,2}$. The electric form factor G_E and the magnetic form factor G_M are functions of Q^2 only, $\tau = Q^2/4m^2$, and $Q^2 > 0$ in the spacelike region. Since the contribution from G_M dominates that of G_E by a factor of τ, and G_E is thought to be small for the neutron, our measurements at large Q^2 are mostly sensitive to G_M.

The experiment was done in End Station A at the Stanford Linear Accelerator Center (SLAC). We detected electrons scattered from 30-cm-long hydrogen or deuterium targets into the 20-GeV/c spectrometer[7] set at 10°. The momentum (E') and polar angle (θ) of the electrons were measured with five planes of multiwire proportional chambers. Electrons were identified in a total-absorption shower counter. We determined the spectrometer acceptance with slits and by collecting over a million events in the deep-inelastic region where the spectrum is flat.

For each incident energy we measured the electron-deuteron and electron-proton cross sections $\sigma(\Omega, E')$ over the entire quasielastic region and well into the inelastic region in eight overlapping steps in spectrometer momentum. The cross sections measured in the overlapped regions were in excellent agreement. High statistics were necessary to determine the precise shapes of the spectra so that we could separate them into elastic and inelastic components. For example, at $Q^2 = 6$ (GeV/c)^2 we collected approximately 6×10^4 e-d events. About 60% of them were in the quasielastic peak region, yielding ~ 3% statistical accuracy in each of 40 bins in E'. The experimental cross sections were radiatively corrected using an iterative method based on the work of Mo and Tsai[8] to get the true cross sections. The cross section at $Q^2 = 6.0$ (GeV/c)^2 is shown as the points in Fig. 1. Notice that the quasielastic peak at $E' = 12.55$ GeV is partly obscured by the inelastic cross section.

As a calibration we compared the elastic e-p cross sections extracted from our hydrogen-target data with previous data at all five values of Q^2. Our results agree with a fit to the world data[10] to within the statistical errors of a few percent.

In the impulse approximation the scattering from deuterium is the sum of scattering from the individual moving nucleons. At our elastic-scattering kinematics this Fermi motion causes a momentum smear of about ± 1.5% full width at half maximum which means that the quasielastic and long tail of the smeared inelastic spectrum overlap at high Q^2. To extract the quasielastic neutron cross section from the deuteron data, the quasielastic proton and smeared inelastic proton and neutron cross sections must be subtracted. The quasielastic neutron cross section is proportional to the smeared elastic proton cross

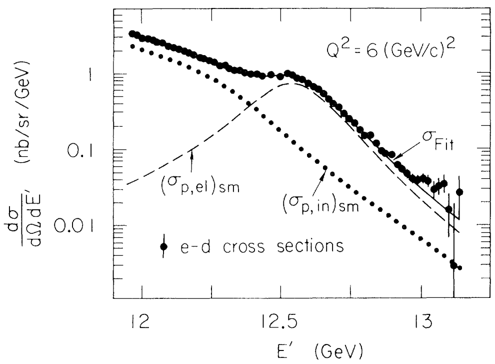

FIG. 1. The cross section for e-d scattering at incident energy $E = 15.742$ GeV vs scattered-electron energy E' at 10°. The dashed (dotted) curve is the smeared elastic (inelastic) e-p cross section obtained with method II and the Paris potential (Ref. 9). The solid curve is the result of a linear least-squares fit of the other two curves to the e-d cross section as described in the text. All cross sections are radiatively corrected.

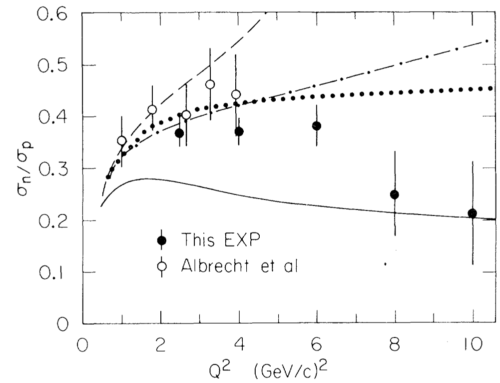

FIG. 2. The ratio σ_n/σ_p as a function of Q^2. Previous data from Albrecht *et al.* (Ref. 6) have been extrapolated to 10°. The dashed and solid curves are the vector-dominance models of Höhler *et al.* and Blatnik and Zovko (Ref. 2), respectively. The dotted curve is form-factor scaling: $G_{Mn}/\mu_n = G_{Mp}/\mu_p = G_{Ep}$ and $G_{En} = 0$. The dash-dotted curve is the dipole law for G_{Mn} with $G_{En} = 0$ and σ_p from our experimental results.

section, $(\sigma_{p,\mathrm{el}})_{\mathrm{sm}}$. The smeared inelastic neutron cross section was assumed to be proportional to the smeared inelastic proton cross section, $(\sigma_{p,\mathrm{in}})_{\mathrm{sm}}$, over our limited range of E'. The smeared proton cross sections were obtained from our hydrogen data supplemented at high inelasticity by the extensive data taken by other groups at SLAC.[11] The Fermi-momentum (p_{F}) distribution was obtained from models[9] of the deuteron wave function.

Two independent methods were used to obtain these smeared proton cross sections. In the first method a Monte Carlo program generated kinematic quantities for elastic and inelastic electrons scattered from moving nucleons. The events were radiated and they were weighted by the deuterium wave function and the cross section. The events were reduced to cross sections by the same procedure as for the real data and then compared with the experimental deuterium cross sections. In the second method we used analytical expressions derived from the work of McGee[12] to calculate the quasielastic and smeared inelastic cross sections. The latter were treated as the sum of narrow elasticlike peaks. These smeared cross sections were compared with the radiatively corrected deuterium cross sections.

In both methods the measured deuterium spectrum was represented by the expression

$$\sigma(\Omega, E') = R_{\mathrm{el}}(\sigma_{p,\mathrm{el}})_{\mathrm{sm}} + R_{\mathrm{in}}(\sigma_{p,\mathrm{in}})_{\mathrm{sm}}.$$

The proportionality constants $R = \sigma_d/\sigma_p = (\sigma_n + \sigma_p)/\sigma_p$ are determined by a least-squares fit. In Fig. 1 the radiatively corrected deuterium spectrum, the quasielastic and smeared inelastic proton spectra, and the fit are shown for $Q^2 = 6.0\ (\mathrm{GeV}/c)^2$.

The good fits at each value of Q^2 support the validity of the assumptions going into the analysis. We studied extensively the sensitivity of the results to various inputs to the analysis and found the largest variations to come from the use of a variety of deuteron wave functions with different high-momentum components for $p_{\mathrm{F}} > 0.25$ GeV/c, and from the two different methods of analysis. The systematic errors are larger than the statistical ones. The errors we present enclose the results for both methods with three different realistic deuteron wave-function models[11]: the

TABLE I. The ratios of elastic electron-neutron to elastic electron-proton cross sections, the values of the neutron cross section, and G_{Mn} extracted from our data using Eq. (1) assuming $G_{En} = 0$. The errors include statistical and systematic effects.

Q^2 $(\mathrm{GeV}/c)^2$	σ_n/σ_p	σ_n (nb)	G_{Mn}
2.5	0.37 ± 0.03	2.9 ± 0.2	0.092 ± 0.004
4.0	0.37 ± 0.03	0.42 ± 0.03	0.041 ± 0.002
6.0	0.38 ± 0.04	0.070 ± 0.007	0.0195 ± 0.0010
8.0	0.25 ± 0.08	0.012 ± 0.004	0.0090 ± 0.0015
10.0	0.21 ± 0.10	0.0031 ± 0.0015	0.0053 ± 0.0013

Paris potential, the Bonn potential, and the Reid soft core modified by recent data of Bernheim *et al.*[13]

Table I lists the ratio $\sigma_n/\sigma_p = R_{el} - 1$, the values of the neutron cross section obtained by using our elastic e-p results for σ_p, and G_{Mn} extracted from Eq. (1) with the assumption $G_{En} = 0$. The ratio σ_n/σ_p is shown in Fig. 2 as a function of Q^2 along with some results from a previous experiment of Albrecht *et al.*[6] Notice that our results are consistent with the other results, but are a little lower. We show the predictions from two commonly used empirical relationships: the dipole law $G_{Mn} = \mu_n/(1+Q^2/0.71)^2$ with σ_p from our data (dash-dotted curve), and form-factor scaling $G_{Mn} = \mu_n G_{Mp}/\mu_p$ (dotted curve), both with $G_{En} = 0$. The dashed curve is the model of Höhler *et al.*[2] which is typical of other vector-dominance model calculations. The new high-Q^2 data fall well below these curves. The solid curve is the vector-dominance model prediction of Blatnik and Zovko[2] which incorporates the asymptotic limits discussed below.

The quark dimensional scaling laws[14] predict that at large Q^2 the spin-averaged hadronic elastic form factor $[A(Q^2)]^{1/2}$ has a power-law dependence $(1/Q^2)^{n-1}$, where n is the number of elementary quark constituents. In Fig. 3 we plot the experimental values $(Q^2)^{n-1}[\sigma/\sigma_M]^{1/2}$ $\{= (Q^2)^{n-1} \times [A(Q^2)]^{1/2}$ at small angles$\}$ versus Q^2 for the pion, the nucleons, and several light nuclei.[15] Within the errors our new neutron form-factor data scale.

Explicit calculations[14] for the nucleon using a model with three spin-$\frac{1}{2}$ quarks show that at large Q^2, $F_1(Q^2) = C_1/(Q^2)^2$ and $F_2(Q^2) = C_2/(Q^2)^3$, where $F_1 = (G_E + \tau G_M)/(1-\tau)$ and $F_2 = (G_E - G_M)/k(\tau - 1)$ are the Dirac and Pauli form factors, and k is the anomalous magnetic moment. The C_1 and C_2 depend on the quark wave function of the nucleons and in particular on the average charge of the leading quark near $x = 1$. If the nucleon wave function is spatially symmetric such that $F_{1n} \to 0$ then $\sigma_n/\sigma_p \to 1/Q^2$ at large Q^2. Alternatively, if the leading quark has the same isospin[15] (helicity[16]) as the nucleon, it follows that $\sigma_n/\sigma_p \to \frac{1}{4}$ ($\frac{1}{9}$). Our results show σ_n/σ_p falling with increasing Q^2 above $Q^2 = 6$ (GeV/c)^2 in a way which is consistent with all three predictions.

There are asymptotic perturbative QCD calculations[4] in which the power-law Q^2 dependence of the form factors given by the dimensional scaling laws (modulo logarithmic corrections) arises from the hard scattering subprocesses involving all the valence quarks. The form factors also depend on the quark wave functions. The calculation of Brodsky and Lepage shows G_{Mn}/G_{Mp} to be particularly sensitive to the wave functions, and for a wide range of possible wave functions they predict $\sigma_n/\sigma_p = (G_{Mn}/G_{Mp})^2 > 1$. This is inconsistent with our results and the trend with increasing Q^2 is in the opposite direction. This could indicate that these asymptotic predictions are not applicable at our Q^2, or that there are some fundamental problems with perturbative QCD. In any case these results will severely restrict models for the nucleon wave functions.

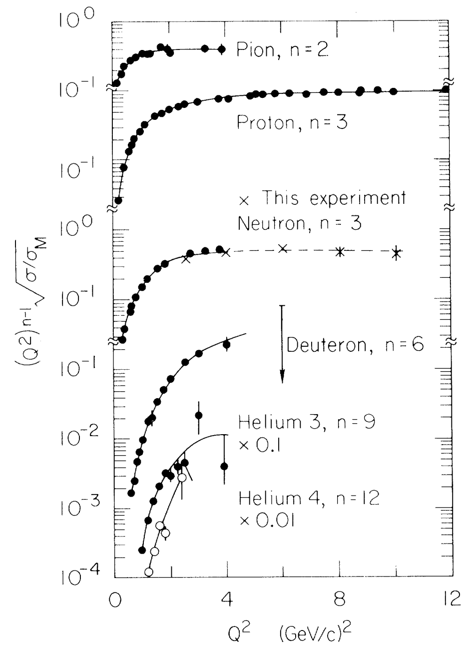

FIG. 3. Quark dimensional scaling of the elastic form factors of the pion, nucleons, and three light nuclei. The power n is the number of elementary quark constituents.

We thank Dave Sherden for his help with our new computer and the Spectrometer Facilities Group for their support. This work was supported by the Department of Energy under Contract No. DE-AC03-76SF00515, and the National Science Foundation under Grants No. PHY78-09378 and No. PHY81-08484.

[a]Deceased.

[b]On leave from Universität Bonn, Bonn, West Germany.

[c]Present address: University of Santiago, Santiago, Chile.

[d]Present address: University of Virginia, Charlottesville, Va. 22903.

[1]T. Narita, Prog. Theor. Phys. 42, 1336 (1969); A. L. Licht and A. Pagnamenta, Phys. Rev. D 4, 2810 (1971).

[2]F. Iachello et al., Phys. Lett. 43B, 191 (1973); S. Blatnik and N. Zovko, Acta Phys. Austriaca 39, 62 (1974); F. Felst, Deutsches Elektronen Synchrotron DESY Report No. 73/56, 1973 (unpublished); G. Höhler et al., Nucl. Phys. B114, 505 (1976).

[3]S. D. Drell and T. M. Yan, Phys. Rev. Lett. 24, 181 (1970); S. J. Brodsky and B. Chertok, Phys. Rev. D 14, 3003 (1976).

[4]S. J. Brodsky and G. P. Lepage, Phys. Scr. 23, 945 (1981); G. P. Lepage and S. J. Brodsky, Phys. Rev. D 22, 2157 (1980).

[5]P. N. Kirk et al., Phys. Rev. D 8, 63 (1973); S. Stein et al., Phys. Rev. D 12, 1884 (1975); W. B. Atwood, Ph.D. thesis, Stanford University, SLAC Report No. 185, 1975 (unpublished).

[6]W. Bartel et al., Nucl. Phys. B58, 429 (1973); K. Hanson et al., Phys. Rev. D 8, 753 (1973); R. J. Budnitz et al., Phys. Rev. 173, 1357 (1968); W. Albrecht et al., Phys. Lett. 26B, 642 (1968).

[7]L. W. Mo, SLAC Report No. SLAC-TN-65-40, 1965 (unpublished); S. Stein et al., Phys. Rev. D 12, 1884 (1975).

[8]L. W. Mo and Y. S. Tsai, Rev. Mod. Phys. 41, 205 (1969); Y. S. Tsai, SLAC Report No. SLAC-PUB-848, 1971 (unpublished).

[9]The Reid potential: R. V. Reid, Jr., Ann. Phys. (N.Y.) 50, 411 (1968). The Bonn potential: K. Holinde and R. Machleidt, Nucl. Phys. A256, 479 (1976). The Paris potential: M. Lacombe et al., Phys. Rev. D 12, 1495 (1975), and Phys. Rev. C 21, 861 (1980).

[10]We use the fit dipole ($\Gamma\rho = 112$ MeV) from Iachello et al., Ref. 2.

[11]A. Bodek et al., Phys. Rev. D 20, 1471 (1979); M. D. Mestayer, Ph.D. thesis, Stanford University, SLAC Report No. 214, 1978 (unpublished); J. S. Poucher et al., SLAC Report No. SLAC-PUB-1309, 1973 (unpublished).

[12]W. Bartel et al., Nucl. Phys. B58, 429 (1973); I. J. McGee, Phys. Rev. 161, 1640 (1967).

[13]M. Bernheim et al., Nucl. Phys. A365, 349 (1981).

[14]S. J. Brodsky and G. Farrar, Phys. Rev. D 11, 1309 (1975).

[15]S. J. Brodsky and B. Chertok, Phys. Rev. D 14, 3003 (1976); and for the He data, R. G. Arnold et al., Phys. Rev. Lett. 40, 1429 (1978).

[16]G. Farrar and D. Jackson, Phys. Rev. Lett. 35, 1416 (1975).

Structure of Single-Particle States in Spherical Nuclei within the Framework of the Multistep Shell-Model Method

R. J. Liotta

Departamento de Física, Comisión Nacional de Energía Atómica, 1429 Buenos Aires, Argentina, and Research Institute of Physics, S-104 05 Stockholm 50, Sweden

and

C. Pomar

Departamento de Física, Comisión Nacional de Energía Atómica, 1429 Buenos Aires, Argentina

(Received 12 July 1982)

The structure of single-particle states in spherical nuclei is analyzed within the shell model by use of a representation which consists of a correlated basis.

PACS numbers: 21.10.Pc, 21.60.Cs

We recently proposed to solve the many-body shell-model equations by means of a representation consisting of many-particle correlated states.[1] In general, a system with a number of particles p can be evaluated in terms of systems with q and r particles, respectively, such that $p=q+r$. One proceeds in several steps. First the one-particle states that span the shell-model space are chosen. In the second step one calculates the two-particle states which define the interaction matrix elements. Then one proceeds by adding particles in successive steps. To evaluate the p-particle system mentioned above, one assumes that the q- and r-particle systems have been solved so that the basis set of elements is given by

$$\{P^\dagger(\alpha_q)P^\dagger(\alpha_r)|0\rangle\}, \tag{1}$$

where $P^\dagger(\alpha_n)$ creates the n-particle state α_n (but, as an exception, the one-particle states are labeled with Latin letters and the corresponding creation operator is $c_i^\dagger$, as usual) and $|0\rangle$ is

